A R C H I V E S O F M E T A L L U R G Y A N D M A T E R I A L S
Volume 59 2014 Issue 3
DOI: 10.2478/amm-2014-0165

I. OLEJARCZYK-WOŻEŃSKA*, H. ADRIAN*, B. MRZYGŁÓD*

MATHEMATICAL MODEL OF THE PROCESS OF PEARLITE AUSTENITIZATION

MATEMATYCZNY MODEL PROCESU AUSTENITYZACJI PERLITU

The paper presents a mathematical model of the pearlite – austenite transformation. The description of this process uses the diffusion mechanism which takes place between the plates of ferrite and cementite (pearlite) as well as austenite. The process of austenite growth was described by means of a system of differential equations solved with the use of the finite difference method. The developed model was implemented in the environment of Delphi 4. The proprietary program allows for the calculation of the rate and time of the transformation at an assumed temperature as well as to determine the TTT diagram for the assigned temperature range.

Keywords: Modelling, phase transformations, TTT diagrams

W pracy zaprezentowano matematyczny model przemiany perlit – austenit. Do opisu tego procesu wykorzystano dyfuzyjny mechanizm zachodzący pomiędzy płytkami ferrytu i cementytu (perlitu) oraz austenitu. Proces wzrostu austenitu opisany został układem równań różniczkowych rozwiązanych przy wykorzystaniu metody różnic skończonych. Opracowany model zaimplementowano w środowisku Delphi 4. Autorski program pozwala na obliczanie szybkości i czasu przemiany przy założonej temperaturze oraz na wyznaczanie wykresu CTP_i dla zadanego zakresu temperatur.

1. Introduction

The modern industry, the continuous technological progress and the continuously increasing requirements of the constructors concerning the material properties create the need to apply computer techniques in the modeling and support of the technological process control [1-11]. Obtaining the desired microstructure of iron-carbon alloys, and thus the appropriate properties, requires the optimization of the technological parameters of the process. That is why, it seems advisable to apply computer techniques which are at present an inexpensive and effective means of optimization in the modeling and support of the heat treatment control.

The proper control of the heat treatment process is especially significant in the case of spheroidal cast iron of a ferrite-austenite structure of the matrix (austempered ductile iron – the so called ADI cast iron). This cast iron characterizes in a favourable combination of high strength, good plasticity and fracture toughness. Due to the properly selected heat treatment, the ADI cast iron can characterize in a strength which exceeds even twice the strength of the normalized types of spheroidal cast iron of the same plasticity [12]. Obtaining a microstructure which combines these properties is, however, a very difficult task. Heat treatment of spheroidal cast iron, which leads to obtaining of a matrix consisting of a mixture of plate ferrite and high-carbon austenite, consists in austenitization and isothermal quenching of the cast iron.

Austenitization, as the first stage of the heat treatment of spheroidal iron casts with the purpose of obtaining the ADI cast iron, consists in heating the casts up to 800-950°C and holding them within the temperature range, in order to obtain an austenite structure of the matrix, which constitutes the starting point for the obtaining of an ausferrite structure [13].

The transformation of pearlite into austenite has a diffusional character. It begins with the nucleation of the austenite at the ferrite-cementite interphase boundaries. The rate of the austenite transformation mostly depends on the heating rate and the general surface of the ferrite-cementite interphase boundaries (pearlite dispersion). In this transformation, we can differentiate between the following stages:

- formation of heterogeneous austenite,
- formation of homogeneous austenite,
- growth of austenite grains.

Directly after the finalization of the pearlite - austenite transformation, the obtained austenite is heterogeneous, and for the full homogenisation of the concentration of carbon and other alloy elements, there is a need for further heating [14].

2. Experimental material and methods

The wide range of mechanical properties of spheroidal ADI cast iron, as it has been mentioned before, is obtained

* AGH UNIVERSITY OF SCIENCE AND TECHNOLOGY, FACULTY OF METALS ENGINEERERING AND INDUSTRIAL COMPUTER SCIENCE, AL. A. MICKIEWICZA 30, 30-059 KRAKÓW, POLAND

due to the properly selected cycle of heat treatment for the formation of the final microstructure determining the quality of the produced cast. This process consists of austenitization and isothermal quenching.

According to the published data [15-18], obtaining the proper austenite microstructure, as the starting point for the ausferrite microstructure, is of essential importance. The temperature and time of austenitization affect the microstructure and initial mechanical properties of the material after the final procedures, that is after the isothermal quenching. Too short a time of austenitization may be the cause of an incomplete transformation of pearlite into austenite, the consequence of which is an un-processed structure adversely affecting the parameters of the ADI cast iron [13, 8-18]. That is why it seems advisable to apply mathematical modeling, the purpose of which is optimizing the technological parameters of the process, such as the temperature and time of austenitization.

2.1. Mathematical model of the process of pearlite-austenite transformation

According to the literature data, we can differentiate between 3 model groups which describe the pearlite (α + Θ where Θ = cementite, Fe_3C) $\rightarrow$ austenite (γ) transformation [17, 19-29]:

- a diffusion mechanism of the transformation which takes place between the ferrite, cementite and austenite plates,
- a diffusion field in the growing austenite grain at the front of the face of the ferrite and cementite plates,
- the Avrami equation (Johnson–Mehl–Avrami equation) of the dependence of a fraction of the transformed austenite on the time.

This work used, adapted and modified the first of the mentioned models.

In the considerations of the model, half of the thickness of a cementite and a ferrite plate was considered, which were conventionally treated in total as the interlamellar distance, x_{perl} (Fig. 1).

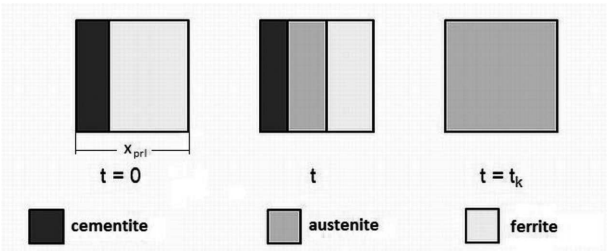

Fig. 1. Scheme of austenitization process [19]

The model makes the following simplifying assumptions:

1. the local equilibrium is obtained at the phase boundaries cementite-austenite (Θ/γ) and austenite-ferrite (γ/α),
2. the equilibrium is considered in the metastable system Fe – Fe_3C – for the purpose of simplification; the substitution element diffusion is omitted,
3. the carbon diffusion in the cementite (stoichiometric phase) is omitted,
4. the effect of the carbon content on the diffusion coefficient in the ferrite is omitted,
5. the effect of the carbon content on the diffusion coefficient in the austenite is considered,
6. the austenite nucleation rate is omitted.

With the assumptions 1-6, the transformation process is controlled by the carbon diffusion in the austenite and ferrite. In the discussed model, the process of austenite growth was described by means of the system of equations (1)-(4) below. The change in the carbon content in the austenite and ferrite in the function of time and distance are presented by equations (1) and (2):

$$\frac{\partial C_\gamma}{\partial t} = D_\gamma \frac{\partial^2 C_\gamma}{\partial x^2} \tag{1}$$

$$\frac{\partial C_\alpha}{\partial t} = D_\alpha \frac{\partial^2 C_\alpha}{\partial x^2} \tag{2}$$

where C_γ, C_α – the carbon content respectively in the austenite and ferrite, mass %, D_γ, D_α – the diffusion coefficients of the carbon in the austenite and ferrite respectively, cm^2/s, t – time, s, and x– distance, cm.

Equations (3) and (4) describe the equilibrium flux of carbon at the interphase boundaries of cementite/austenite (Θ/γ) and austenite/ferrite (γ/α), respectively, and they make it possible to determine the rate of the phase boundary migration:

$$V_{\Theta\gamma}\left(C_\Theta \rho_\Theta - C_\gamma^{\gamma\Theta}\rho_\gamma\right) = D_\gamma \rho_\gamma \left(\frac{\partial C_\gamma}{\partial x}\right)_{x=x^+_{\Theta\gamma}} \tag{3}$$

$$V_{\gamma\alpha}\left(C_\gamma^{\gamma\alpha}\rho_\gamma - C_\alpha^{\gamma\alpha}\rho_\alpha\right) = -D_\gamma \rho_\gamma \left(\frac{\partial C_\gamma}{\partial x}\right)_{x=x^+_{\gamma\alpha}} + D_\alpha \rho_\alpha \left(\frac{\partial C_\alpha}{\partial x}\right)_{x=x^-_{\gamma\alpha}} \tag{4}$$

where: $V_{\Theta\gamma}$ and $V_{\gamma\alpha}$ – the rate of the migration of the phase boundaries cementite – austenite (Θ/γ) and austenite – ferrite (γ/α), in cm/s, ρ_γ – the austenite density, ρ_Θ – the cementite density, ρ_α – the ferrite density, in g/cm^3, $C_\gamma^{\gamma\Theta}$, $C_\gamma^{\gamma\alpha}$ – carbon contents in austenite at interphase boundaries austenite – cementite and austenite – ferrite respectively, $C_\alpha^{\gamma\alpha}$ – in ferrite at interphase boundary austenite – ferrite and C_Θ – carbon content in cementite, in mass %.

To the initial conditions belong: the initial thicknesses of the plates of cementite, l_Θ, ferrite, l_{fer}, and austenite, l_a, (at start point assumed $l_a = 10^{-5} l_\Theta$). The initial carbon contents in the particular phases are presented by equation (5), whereas those at the phase boundaries – by equations (6) and (7).

$$\begin{aligned} C &= C_\Theta \quad \text{for} \quad 0 \leqslant x \leqslant l_\Theta \\ C &= C_\alpha \quad \text{for} \quad l_a \leqslant x \leqslant x_{perl} \\ C &= f(x) \quad \text{for} \quad l_\Theta \leqslant x \leqslant l_a \end{aligned} \tag{5}$$

$$\begin{aligned} C_\gamma &= C_\gamma^{\gamma\Theta} \quad \text{for} \quad x = x^+_{\Theta\gamma} \\ C_\gamma &= C_\gamma^{\gamma\alpha} \quad \text{for} \quad x = x^-_{\gamma\alpha} \end{aligned} \tag{6}$$

$$\frac{\partial C_\alpha}{\partial x_{x=x_{perl}}} = 0 \tag{7}$$

2.2. Numerical solution

Between the interfacial surfaces Θ/γ and γ/α, a uniform lattice of nodes M was introduced, by way of dividing the austenite area into M-1 segments of the initial length of $\Delta x = l_a/(M-1)$. In an analogous manner, the lattice of nodes M_1 was applied on the ferrite area (Fig. 2).

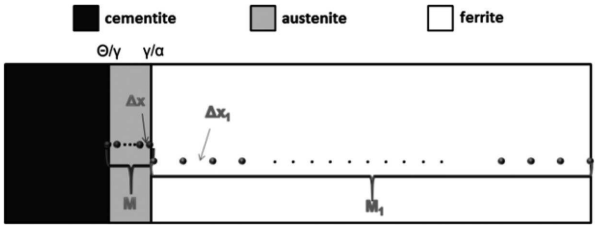

Fig. 2. Scheme of a nodes lattice in austenite and ferrite

Equations (1) and (2) describing the change of the carbon content in the austenite and ferrite were solved with the use of the finite difference method. In the course of the calculations, the number of nodes remains the same, whereas the distance between them changes. In order to consider the movement of the nodes in the function of time, the varying Murray-Landis lattice was applied [30]. To that end, in the equations for the change in the carbon content, the movement rate of m and m_1-nodes was introduced (V_m, V_{m1}). The difference form (explicite discretization) of the changes in the carbon content in the austenite and ferrite are presented by equations (8) and (9):

$$\frac{C_{\gamma m}^{j+1} - C_{\gamma m}^{j}}{\Delta t} = D_\gamma \left(\frac{C_{\gamma m+1}^{j} - 2C_{\gamma m}^{j} + C_{\gamma m-1}^{j}}{\Delta x^2} \right) + V_{\gamma m} \left(\frac{C_{\gamma m+1}^{j} - C_{\gamma m-1}^{j}}{2\Delta x} \right) \tag{8}$$

$$\frac{C_{\alpha m1}^{j+1} - C_{\alpha m1}^{j}}{\Delta t} = D_\alpha \left(\frac{C_{\alpha m1+1}^{j} - 2C_{\alpha m1}^{j} + C_{\alpha m1-1}^{j}}{\Delta x_1^2} \right) + V_{\alpha m} \left(\frac{C_{\alpha m1+1}^{j} - C_{\alpha m1-1}^{j}}{2\Delta x_1} \right) \tag{9}$$

Where m and $m1$ are numbers of successive node in austenite and ferrite respectively, and j is the time step.

The rate of the lattice node movement in the austenite is presented by formula (10), whereas that in the ferrite – formula (11):

$$V_{\gamma m} = \frac{x_{\gamma\alpha} - x}{x_{\gamma\alpha} - x_{\Theta\gamma}} V_{\Theta\gamma} + \frac{x - x_{\Theta\gamma}}{x_{\gamma\alpha} - x_{\Theta\gamma}} V_{\gamma\alpha} \tag{10}$$

$$V_{\alpha m1} = \frac{x_{perl} - x}{x_{perl} - x_{\gamma\alpha}} V_{\gamma\alpha} \tag{11}$$

where: x – the location of the current point, $x_{\gamma\alpha}$ – the location of the austenite/ferrite interphase boundary, $x_{\Theta\gamma}$ – the location of the cementite/austenite interphase boundary.

The balance equations of the carbon mass at the interphase boundaries cementite/austenite and austenite/ferrite were calculated with the use of the symmetric difference quotient (equations (12) and (13):

$$V_{\Theta\gamma} \left(C_\Theta \rho_\Theta - C_\gamma^{\gamma\Theta} \rho_\gamma \right) = D_\gamma \rho_\gamma \left(\frac{-3C_{m=1} + 4C_{m=2} - 3C_{m=3}}{2\Delta x} \right) \tag{12}$$

$$V_{\gamma\alpha} \left(C_\gamma^{\gamma\alpha} \rho_\gamma - C_\alpha^{\gamma\alpha} \rho_\alpha \right) = -D_\gamma \rho_\gamma \left(\frac{C_{M-2} - 4C_{M-1} + 3C_M}{2\Delta x} \right) + D_\alpha \gamma_\alpha \left(\frac{-3C_{m1=1} + 4C_{m1=2} - C_{m1=3}}{2\Delta x_1} \right) \tag{13}$$

Using the informations on the position of nodes on interphase boundaries the actual thickness of cementite, l_Θ, ferrite, l_{fer}, and austenite, l_a, were calculated.

2.3. Physical data

Exemplary calculations were performed at two different initial interlamellar distances: 0,1μm and 1 μm. On the basis of the diagram Fe – Fe_3C, with the use of the lever rule, it was assumed that the ratio of the ferrite plate thickness to the cementite plate thickness equals 7,68. In the calculations, a temperature dependence of the diffusion coefficient of carbon in the ferrite was assumed, on the basis of [13] (equations (14)):

$$D_\alpha = 7,90 \cdot 10^{-3} \exp\left(\frac{-7,58 \cdot 10^4}{RT} \right) \tag{14}$$

where: R – the gas constant, in J/(mol K), T – the temperature in K, and the coefficient D_α – cm^2/s.

The diffusion coefficient of carbon in austenite was calculated with consideration of the temperature and the carbon content effects, D_γ(C,T). In the determination of D_γ the Siller and McLellan method, adopted by Bhadeshia [33], was applied [31,32]. According to Siller and McLellan [31,32], the coefficient $D_\gamma(C,T)$ is expressed by means of equation (15):

$$D_\gamma (C,T) = D' \xi (C_a) \tag{15}$$

where: C_a – the atomic fraction of carbon, D' – the coefficient dependent on temperature and independent of the carbon content, described by means of equation (16):

$$D' = \frac{kT}{h} \exp\left(-\frac{\Delta F^*}{kT} \right) \left(\frac{\lambda^2}{3\gamma_m} \right) \tag{16}$$

where: k – the Boltzmann constant, h – the Planck constant, ΔF^* – the activation free energy, independent of the chemical composition and temperature, γ_m – the activity coefficient of the "active complex" in austenite, a constant value, λ – the distance between the austenite crystallographic planes, {002}.

By way of using the quasi-chemical thermodynamic model of the first order for the carbon in the austenite as well as the reaction rate theory, Siller and McLellan presented the part of equation (15) dependent on the carbon concentration (17):

$$\xi (C_a) = \alpha \left(1 + \frac{z(1 + C_a)}{1 - \left(\frac{z}{2} + 1 \right) + \frac{z}{2} \left(\frac{z}{2} + 1 \right) (1 - \sigma) C_a^2} \right) + (1 + C_a) \frac{d\alpha}{dC_a} \tag{17}$$

where σ is given by equation (18):

$$\sigma = 1 - \exp\left(-\frac{\Delta \varepsilon}{kT} \right) \tag{18}$$

and: z – the coordination number of the octahedral voids in the austenite lattice, α – the carbon activity in austenite, $\Delta\varepsilon$ – the energy of repulsion of neighbouring carbon atoms, equaling 8250J/mol.

By way of using the experimental data, it was proven that $(\Delta F^*/k)$ =21230K and $ln(3\gamma_m/\lambda^2)$ =31,84 [31,32].

Fig. 3 shows the dependence of the diffusion coefficient of carbon in austenite, $D_\gamma(C,T)$, on the carbon content at two temperatures: 750°C and 850°C.

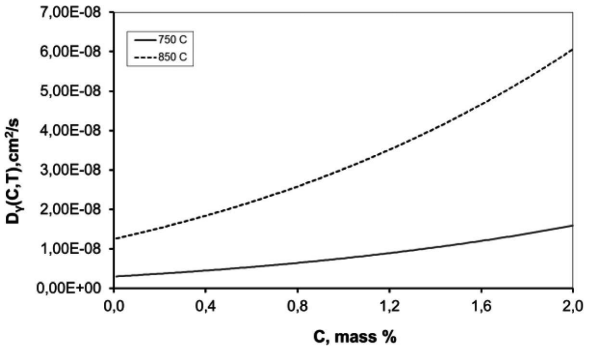

Fig. 3. Dependence of the diffusion coefficient of carbon in austenite on the carbon content at two temperatures: 750°C and 850°C

The carbon content at the boundaries cementite/austenite, austenite/ferrite and ferrite/austenite were determined on the basis of the phase metastable equilibrium system Fe – Fe_3C by way of digitalizing the lines SE (A_{cm}), GS (A_{c3}) and the GP, with the use of the SigmaScanPro5 software [34]. The dependences of temperatures on the carbon content are presented in equations (19)-(21):

$$T_{SE} = -66,40491C^4+421,293C^3-1027,347C^2+1426,765C+69, \quad (19)$$

$$T_{GS} = -2236,709C^5 + 525,0694C^4 - 4682,565C^3 + 2098,812C^2 - 690,06980C + 911,5657 \quad (20)$$

$$T_{GP} = -8486,24C + 912 \quad (21)$$

where: C – the carbon content, mass %.

In the initial stage (for time t=0), the austenite γ does not exist; however, for the numerical purpose, it is assumed that the thickness of the austenite plate equals 0,00001 of the thickness of the cementite plate. In the austenite and ferrite areas, identical number lattices nodes were applied ($M = M_1 = 100$).

2.4. Computer program

The discussed mathematical model of the transformation of pearlite into austenite was implemented in the Pascal computer language, in the Delphi 4 environment.

The program windows for pearlite-austenite calculations is shown in Fig. 4.

The program provides for 2 calculation variants:

- variant I – for the assigned temperature, it allows for the calculation of the rate of the austenite growth and the ferrite and cementite decay, as well as the growth of the austenite plate thickness and the ferrite and cementite decay (Fig. 4a),
- variant II – it allows for the determination of the isothermal time – temperature - transformation, TTT diagram, for the assigned temperature range (Fig. 4b).

Besides the diagrams, the calculation data is saved in a file.

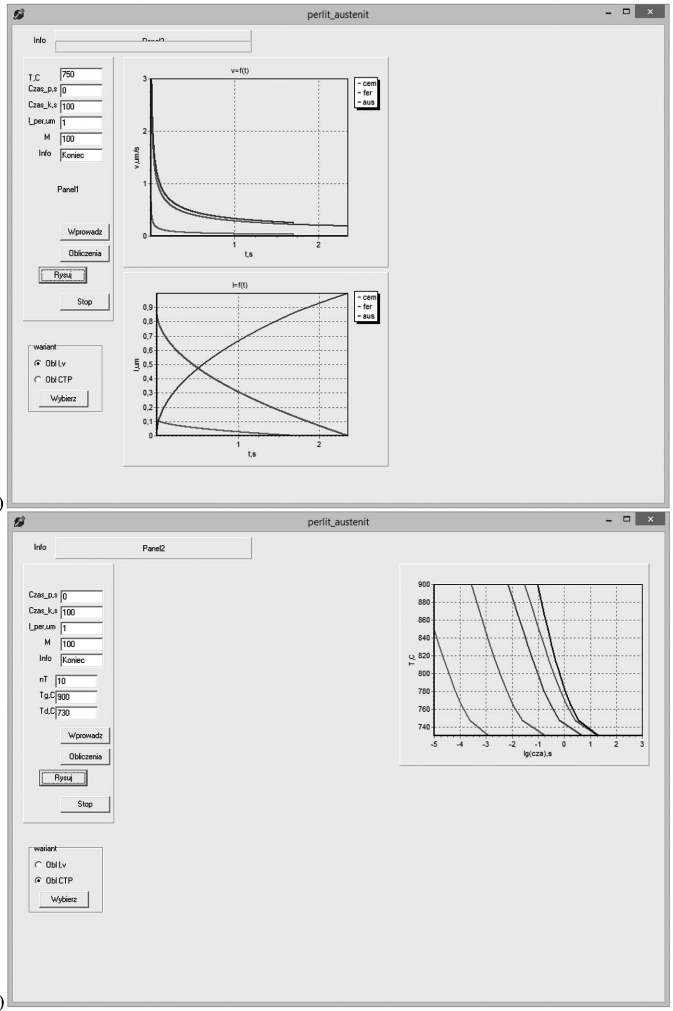

Fig. 4. Program windows a) I calculation variant, b) II calculation variant

3. Results and discussion

With the use of the developed program, we analyzed the effect of the initial thickness of the pearlite plates (interlammellar distance) and of the temperature on the rate of the pearlite into the austenite transformation. The calculation results are presented in Figs. 5 and 6.

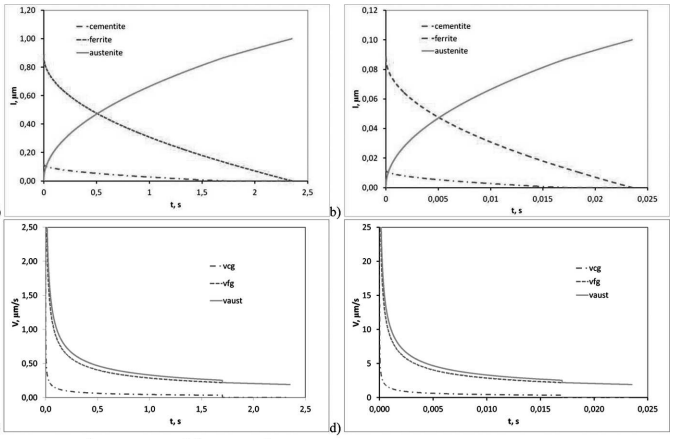

Fig. 5. Time dependence of the austenite, cementite and ferrite plate thickness, l, and the rate, v, of changes during transformation at 750°C, for the interlamellar distances: a), c) – 1 μ m, b), d) – 0,1 μm

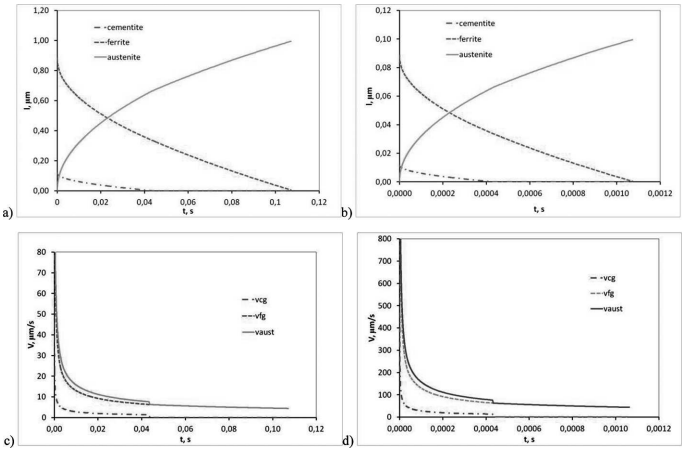

Fig. 6. Time dependence of the austenite, cementite and ferrite plate thickness, l, and the rate, v, of changes during transformation at 850°C, for the interlamellar distances: a), c) – 1 μm, b), d) – 0,1 μm

Sections of the TTT diagrams (second calculation variant in Fig. 4) are presented in Fig. 7, where appropriate lines refer to different volume fraction, V_v of the transformed austenite, from 1 to 99% .

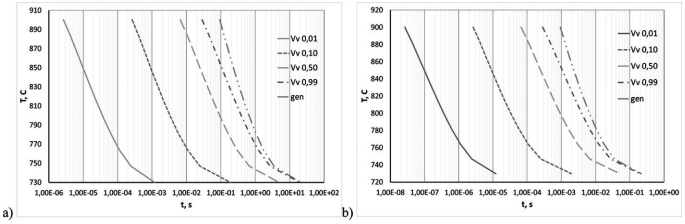

Fig. 7. The calculated TTT diagrams, for: a) interlamellar distance - 1 μm, b) interlamellar distance – 0,1 μm

4. Concluding remarks

The pearlite – austenite transformation is a diffusional transformation. It occurs in two stages. The first stage is the formation of austenite nuclei. The second stage involves the growth of the austenite nuclei up to the moment of a complete transformation of the pearlite into austenite. And so, the transformation rate depends on the rate of the austenite grain nucleation and on the growth rate as well. Both of these transformation parameters depend on the temperature and chemical composition of the alloy. The presented model of the pearlite – austenite transformation is a simplified one. It refers to the second stage – the growth after the nucleus formation only. That is why the times of the transformation finalization calculated with the use of the developed program at a given temperature (after the complete disappear of the ferrite and cementite and the homogenization of the chemical composition of the formed austenite plate) are shorter than the times determined experimentally and presented in empirical TTT diagrams [35]. The obtained results, however, make it possible to perform a qualitative analysis of the effect of the pearlite interlamellar distance as well as the transformation temperature on the relative transformation time.

The work analyzes the effect of the pearlite interlamellar distance on the rate of the ferrite and cementite plate disappear and on the growth of the thickness of the forming austenite plate, on the example of two assumed interlamellar distances: 0,1μm and 1μm.

The results of the analysis point to the fact that the thickness of the ferrite and cementite plates strongly affect the transformation time at a given temperature. In the case of the interlamellar distance equaling 1μm, the remaining time before the finalization of the transformation is longer than the transformation time of the pearlite with the interlamellar distance of 0,1μm, by two orders of magnitude.

The obtained and presented results are in accordance with the results published in [18-22].

Further examinations and modification of the computer program will aim at considering the nucleation rate, the effect of the carbon content on the diffusion coefficient, the chemical composition and the calculation of the continuous- cooling – transformation, CCT diagram.

Acknowledgements

The financial support within the project NCN no. N N508 792440 is gratefully acknowledged.

REFERENCES

[1] H. Adrian, Numeryczne modelowanie procesów obróbki cieplnej, Wydawnictwa AGH, Kraków 2011.
[2] J. Krawczyk, H. Adrian, The kinetics of austenite grain growth in steel for wind power plant shafts, Archives of Metallurgy and Materials **55**, 91-100 (2010).
[3] H. Adrian, E. Głowacz, The effect of nitrogen and microalloying elements (V and V+Al) on austenite grain growth of 40Cr8 steel, Archives of Metallurgy and Materials **55**, 107-1116 (2010).
[4] I. Olejarczyk, A. Adrian, H. Adrian, B. Mrzygłód, Algorithm for control of quenching process of constructional steels, Archives of Metallurgy and Materials **55**, 171-179 (2010).
[5] P. Skubisz, H. Adrian, J. Sińczak, Controlled cooling of drop forged microalloyed-steel automotive crankshaft, Archives of Metallurgy and Materials **56**, 93-107 (2011).
[6] I. Olejarczyk-Wożeńska, A. Adrian, H. Adrian, B. Mrzygłód, Parametric representation of TTT diagrams of ADI cast iron, Archives of Metallurgy and Materials **57**, 621-625 (2012).
[7] H. Adrian, M. Pelczar, A. Adrian, J. Augustyn-Pieniążek, The effect of B and microalloying elements (V, Ti, Nb) additions on the austenite grain growth of low alloy steel, Solid State Phenomena **197**, 25-32 (2013).
[8] E. Głowacz, H. Adrian, W. Osuch, Nitrogen content effect on carbonitride coagulation in 40Cr8 steel with micro-additions V and V+Al, Archives of Metallurgy and Materials **59**, 609-613 (2013).
[9] M. Głowacki, Modelowanie matematyczne i symulacje komputerowe odkształcania metali. Teoria i praktyka, Wydawnictwa AGH, Kraków 2012.
[10] M. Hojny, Application of an integrated CAD/CAM/CAE/IBC system in the stamping process of a bathtub 1200 S, Archives of Metallurgy and Materials **55**(3), 713-723 (2010).
[11] Z. Górny, S. Kluska-Nawarecka, D. Wilk-Kolodziejczyk, Heuristic models of the toughening process to improve the properties of non-ferrous

metal alloys, Archives of Metallurgy and Materials **58**, 849-852 (2013).
[12] C. Podrzucki, Żeliwo. Struktura, własności, zastosowanie, t.I i II, Wyd ZG STOP, Kraków 1991.
[13] W. Kapturkiewicz, Modelowanie kinetyki austenityzacji żeliwa sferoidalnego perlitycznego, Archives of Foundry **4**, 203-208 (2004).
[14] J. Pacyna [pod red.], Metaloznawstwo wybrane zagadnienia, WND AGH, Kraków 2005.
[15] J. Achary, D. Venugopalan, Metall. Mater. Trans. **31A**, 2575-2585 (2000).
[16] A. Ali, R. Elliott, Mater. Sci. Technol. **12**, 1021-1031 (1996).
[17] M. Ahmadabadi, M. Parsa, Mater. Sci. Technol. **17**, 162-167 (2001).
[18] S. Yazdani, R. Elliott, Mater. Sci. Technol. **15**, 541-546 (1999).
[19] T. Akbay, R. Reed, C. Atkinson, Acta Metall. Mater. **42**, 1469-1480 (1994).
[20] C. Atkinson, T. Akbay, R. Reed, Acta Metall. Mater. **43**, 2013-2031 (1995).
[21] C. Atkinson, T. Akbay, Acta Mater. **44**, 2861-2868 (1996).
[22] R. Mancini, C. Budde, Acta Mater. **47**, 2907-2911 (1999).
[23] F. Caballero, C. Capdevila, C. Garcia de Andres, Scripta Mater. **42**, 1159-1165 (2000).
[24] A. Jacot, M. Rapaz, Acta Mater. **45**, 575-585 (1997).
[25] A. Jacot, M. Rapaz, R. Reed, Acta Mater. **46**, 3949-3962 (1998).
[26] D. Gaude-Fugarolas, H. Bhadeshia, J. Mat. Sci. **38**, 1195-1201 (2003).
[27] J. Elmer, T. Palmer, W. Zhang, B. Wood, T. DebRoy, Acta Mater. **51**, 3333-3349 (2003).
[28] T. Szeng, G. Shi, Mater. Sci. Eng. A **380**, 123-136 (2004).
[29] A. Kumar, S. Misra, J. Elmer, T. Debroy, Metall. Mater. Trans. **36A**, 15-22 (2005).
[30] D. Murray, F. Landis, Trans. Am. Soc. Min. Engrs **81**, 106 (1959).
[31] R. Siller, R. McLellan, Trans. Am. Inst. Min. Engrs **245**, 697 (1969).
[32] R. Siller, R. McLellan, Trans. Am. Inst. Min. Engrs **1**, 985 (1970).
[33] H. Bhadeshia, Metal Sci. **15**, 477 (1981).
[34] SigmaScan Pro Automated Image Analysis Software, User's Manual, Jandel Scientific Software, 1995.
[35] K.E. Thelning, Steel and its Heat Treatment, Butterwords, 1984.

Received: 10 January 2014.